Magnet System of the New Electron Cooler for the CERN Antiproton Decelerator (AD) Ring

L. von Freeden, D. Schoerling, and M. Karppinen

***Abstract*—A new electron cooler for the Antiproton Decelerator (AD) ring at CERN is under construction and will be installed in the next long shutdown (2026-2028) to replace the existing 40-year-old device. This paper presents the design of the new electron cooler's normal conducting magnet system comprising three straight solenoid sections joined by two toroidal field sections. Compared to the existing electron cooler magnet system, the new magnet system gives a factor five improvement of cooling region field quality. The field correction scheme used to achieve this improvement will be discussed in detail. The upgrade has the potential to reduce the length of the electron cooling plateaus in the AD cycle and thereby increase the number of antiprotons available to CERN's rich antimatter physics program.**

***Index Terms*—antiproton, electron cooling, solenoid field correction.**

I. Introduction

The AD ring uses electron cooling for beam conditioning at two plateaus, 300 MeV c^{-1} and 100 MeV c^{-1}. The magnet system of the present AD electron cooler was originally built in the 1970 s for the Initial Cooling Experiment (ICE), later repurposed for the Low Energy Antiproton Ring (LEAR), and then finally installed into the AD ring. The age of the electron cooler system and the difficulties in procuring spare parts led to a consolidation review in 2019. The review recommended the construction of a completely new electron cooler, scheduled for installation during the third long shutdown of the CERN accelerator complex (LS3).

The new magnet system is currently under construction to be ready for installation in the final quarter of 2026. This paper presents the design and specification of the new magnet system. A comprehensive discussion on the system level specification of the new electron cooler is provided in [1], and the parameters most relevant to the magnet system are summarized in Table I. In addition to improved reliability, the consolidation provides the opportunity to increase the cooling performance. The key improvements are: the ability to switch off the electron beam during energy ramps; the addition of beam expansion to reduce the electron beam's transverse temperature; and improved field quality in the cooling region. In electron cooler magnet systems, the field quality is defined by

TABLE I
Summary of the Parameters of the New AD Electron Cooler

Parameter	Units	Value	
AD cooling plateaus	MeV c^{-1}	100	300
Electron energies	keV	2.9	25.5
Electron beam currents	A	0.1	2.4
Magnetic field at gun	mT	240	
Magnetic field in cooling region	mT	60	
Field quality in cooling region		$<2\times10^{-4}$	
Length of cooling region	mm	950	
Beam radius in cooling region	mm	25	
Angle of toroidal region	°	36	
Radius of toroidal region	mm	1000	

$$f_q = \left|\frac{B_\perp}{B_{||}}\right| \quad (1)$$

where $B_{||}$ is the magnetic field in the direction parallel to the reference trajectory, and $B_\perp$ is the magnetic field perpendicular to the reference trajectory. The most recent measurements of the AD electron cooler magnet system measured field errors up to 2×10^{-3} in a Ø56 mm × 1 m cooling region [2].

II. Principles of Electron Cooling

In electron cooling, an electron beam with the same average velocity is merged with the antiproton beam. The electron beam has a lower momentum spread than the antiproton beam and is continually replenished. Coulomb interactions between the two beams lead to a net reduction in the antiprotons' momentum spread, "cooling" the beam. The electrons are contained in a solenoidal field to guide them from the electron gun, into the antiproton beam and then to a collector. As the electrons are following the magnetic field lines, the apparent temperature of the electrons is a combination of both their temperature and the field straightness in the cooling region.

Beam expansion makes use of the phenomenon that as electrons pass along a negative field gradient their cyclotron motion slows [3]. A negative field gradient is achieved by placing the electron gun in a higher magnetic field than that of the cooling region. If the field gradient is too large, the magnetic moment is not conserved and the expansion of the electron beam is non-adiabatic. Non-adiabatic expansion results in a less effective reduction, or even an increase, in electron temperature. In [4], the adiabatic parameter is introduced that compares the helical

Received 28 July 2025; revised 20 September 2025; accepted 25 September 2025. Date of publication 1 October 2025; date of current version 13 October 2025. *(Corresponding author: L. von Freeden.)*

The authors are with CERN, 1211 Geneva, Switzerland (e-mail: luke.von.freeden@cern.ch).

Color versions of one or more figures in this article are available at https://doi.org/10.1109/TASC.2025.3615919.

Digital Object Identifier 10.1109/TASC.2025.3615919

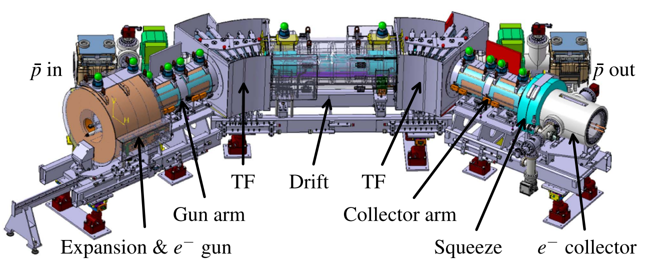

Fig. 1. Full magnet system with sub-elements labeled. The antiprotons, $\bar{p}$, travel from left to right. The electrons, e^-, travel from the gun to the collector.

TABLE II
SUMMARY OF THE ELEMENTS OF THE MAGNET SYSTEM.

Type	Turns	Conductor (mm × mm)	Inner dim. (mm)	Length (mm)	Mass (kg)
Drift	300	9 × 10, ⌀6	⌀403	1505	1180
Arm	41	9 × 10, ⌀6	⌀282	430	178
TF large	64	5.6 × 6.4, ⌀3	600 × 400	62	42
TF small	64	5.6 × 6.4, ⌀3	380 × 400	62	35
Expansion	1440	9 × 9, ⌀6	⌀400	712	2610
Squeeze	484	8.5 × 8.5, ⌀5.5	⌀254	234	510

Hollow conductor dimensions: axial width × radial height, tube diameter.

pitch of the electron's trajectory, λ_c, to the characteristic length scale of magnetic field variation, L_B. The adiabatic parameter is given by

$$\chi = \underbrace{\frac{2\pi\sqrt{2m_e E_e}}{eB}}_{\lambda_c} \cdot \underbrace{\frac{1}{B}\left|\frac{dB}{ds}\right|}_{1/L_B} \tag{2}$$

where m_e is the mass of an electron, E_e is the energy of the electrons, e is the charge of an electron, B is the magnetic field, and s is distance along the beam trajectory. To satisfy the adiabatic condition, $\chi \ll 1$ [4].

III. Specification of the Main Magnet System

The proposed magnet system is shown in Fig. 1, and the specifications of the coil types are given in Table II.

In the center of the device, there is the drift solenoid. The main winding of the drift solenoid has two layers, each wound from a continuous length of conductor. The drift solenoid is fitted with 16 saddle coil pairs and 2 solenoid windings for field correction, and 2 saddle coil pairs for steering the electron beam. All of the coils are impregnated into a 10 mm thick steel tube to provide magnetic shielding and flux return. Once impregnated, the drift is a single rigid body.

Either side of the drift there are toroidal field (TF) regions. Each TF region consists of three large and three small racetrack coils. The coils are equally spaced along a 36° arc with radius 1m. Two coil sizes are used to facilitate integration with the vacuum chamber. The impregnated coils have features banded and bonded onto the outside for assembly.

Outside of the TF sections there are the arms, collector side and gun side. The arms are split to allow a vacuum support to pass through. The arm solenoids are constructed in a similar way to the drift solenoid. They contain two pairs of saddle coils for steering the electron beam.

At the end of the gun arm there is the expansion solenoid to provide a higher magnetic field around the gun. The expansion solenoid is formed of four coils mounted into a 25 mm thick yoke.

At the end of the collector solenoid is the squeeze coil. The squeeze coil boosts the magnetic field, reducing the beam size to pass the collector's entrance electrode. The squeeze coil is constructed in a similar way to the TF coils.

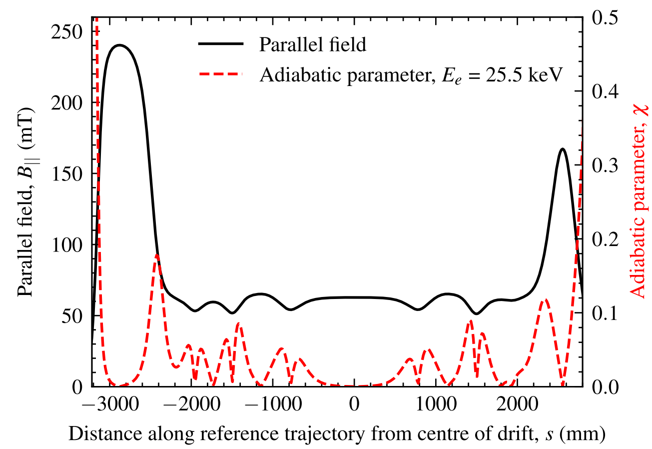

Fig. 2. Computed field along the electron reference trajectory and adiabatic parameter, as defined in (2), for the $E_e = 25.5$ ke V case.

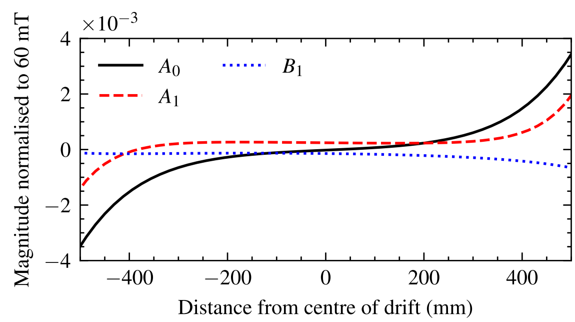

Fig. 3. Normalized Fourier coefficients of the computed radial field in the drift before correction. Computed at a radius of 30 mm.

IV. Design and Simulation

Opera 3D [5] was used to compute the magnetic field produced by the magnet system. The field along the electron reference trajectory and the adiabatic parameter is shown in Fig. 2. The Fourier coefficients of the radial field error are shown in Fig. 3. In the presence of axial field it is not valid to scale to other radii, and these coefficients are not to be confused with the multipole expansion typically quoted for accelerator magnets. In the cooling region, there are three types of systematic field error that are significant in the 1×10^{-4} range. The largest contribution is from solenoidal field (3.5×10^{-3}, constant with angle, A_0). It is an artifact of the gap between the drift solenoid and the TF region to provide clearance for a vacuum flange connection. The second largest is horizontal dipolar field (1.5×10^{-3}, cosine-like, A_1), and is due to the curve artifact of the TF region extending into the drift solenoid. The third largest is vertical dipolar field (0.5×10^{-3}, sine-like, B_1), and is due to up-down asymmetries in the mechanical design of the shielding structures.

A. Field Correction Approach

Solenoidal field errors are corrected using additional windings placed at the extremities of the drift region. These correction coils are located as close as possible to the region where turns are missing, without violating integration constraints. However, a displaced coil cannot exactly reproduce the field of the missing turns. The correction therefore represents the best feasible approximation.

The correction of the dipolar errors in electron coolers is typically performed using one of two approaches. The first involves making the drift solenoid from a series of shorter solenoids (pancake coils), whose angles are then adjusted to minimize dipolar artifacts. For example, in the electron cooler installed in the Low Energy Ion Ring (LEIR) at CERN, an on-axis field quality of 2×10^{-4} was achieved over the central 1.9 m of a 2.5 m drift after five iterations of coil adjustment [6].

The second approach uses dedicated dipole correctors, typically saddle coils, in the drift. For example, in the electron cooler installed in the Extra Low Energy Antiproton Ring (ELENA) at CERN, an on-axis field quality of 5×10^{-4} was achieved over the central 0.6m of a 1m drift [7]. Similar correction strategies have been employed in the electron coolers of the Fermilab (FNAL) Recycler Ring [8] and the High Intensity heavy-ion Accelerator Facility (HIAF) spectrometer ring (SRing) [9], where correction coils are used but the main solenoid is still made in sections for practical reasons.

For the present design, both options were considered in detail before selecting saddle coils as the most suitable solution. The electron cooler cannot be measured in situ or with the vacuum system installed. This limitation implies that the system must be measured and corrected in the lab, and subsequently reassembled into the accelerator with the vacuum system. Therefore, it is essential that the correction scheme not only achieves the required field quality but is also reproducible after reassembly.

In the pancake coil case, it was considered that the coil position could be controlled with a tolerance of 0.2 mm (3σ, normally distributed) at the location of the survey targets. The angular tolerance is a non-linear combination of three positional tolerances and the transverse field contributions from each coil overlap. Due to this complexity, numerical methods where used to study the tolerance stack up from the correction scheme to the field quality in the cooling region. A Monte Carlo analysis with 5×10^5 seeds was performed and the resulting distribution of field quality deviations is shown in Fig. 4. The mean change in field quality is 1.9×10^{-4} and the 3σ upper bound is 3.5×10^{-4}.

In the saddle coil correction scheme proposed, it is possible to control the current to a tolerance of 300 ppm (3σ, normally distributed) considering long term drift, resolution, and ripple. These result in a mean field quality deviation of 1.4×10^{-6} and a 3σ upper bound of 2.5×10^{-6} for the correction scheme alone. There is cross talk from the TF regions into the cooling region.

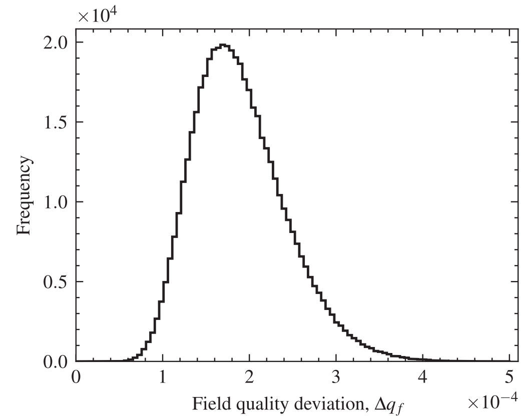

Fig. 4. Distribution of change in field quality due to the tolerance on coil positioning in the rejected coil rotation correction scheme for 5×10^5 coolers.

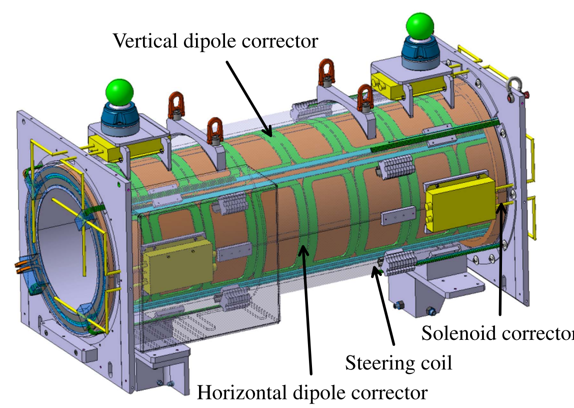

Fig. 5. Drift solenoid with the main shielding hidden to show the correction coil scheme.

Therefore, the sensitivity of the field quality to tolerance of the position and powering of the TF regions has also been considered. Combining the tolerance of both the correction scheme and the TF regions, it is expected that the field quality measured in the lab can be reproduced within 3.3×10^{-5} in the accelerator.

There were two possible correction coil layouts found that gave satisfactory field quality in the cooling region. The first uses six coils concentrated at the ends of the drift solenoid, the region with more interference from the TF regions. The layout finally selected uses eight coils that are evenly spaced along the drift as it is more robust to correct random errors arising during manufacturing. An image of the drift solenoid with the correction coils is shown in Fig. 5.

B. Correction Strengths

There is negligible cross talk between the solenoidal, and horizontal and vertical dipole correction schemes so all three can be considered separately. The steel is far from saturation, so the superposition of the correctors is close to linear. As a result, the design of the correction strengths can be formulated into a linear algebra expression [10]. For each of the three correction types, a matrix equation is set up by considering m evenly spaced points in the cooling region. First, the field error at these points

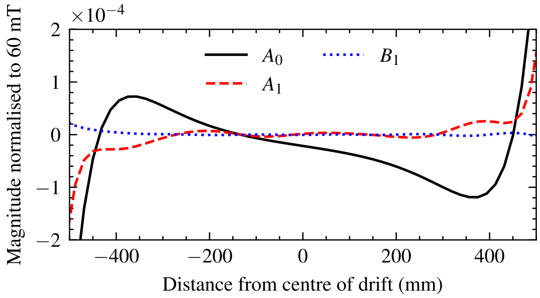

Fig. 6. Normalized Fourier coefficients of the computed radial field in the drift after application of the correction scheme found using (4). Computed at a radius of 30 mm.

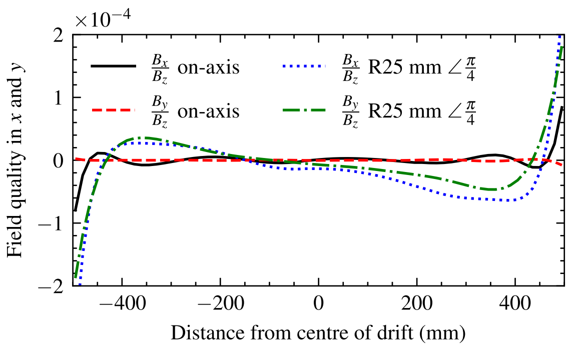

Fig. 7. Computed field quality after the application of the correction scheme found using (4). The off-axis values are given at a radius, R, of 25 mm and an angle, $\angle$, of $\frac{\pi}{4}$ from the x-axis.

is sampled to create an error vector, $\vec{e}$, length m. Secondly, we sample the transfer function of field contributions given by the n relevant correctors and store them in vectors $\vec{c_0}, \vec{c_1}, \ldots, \vec{c_n}$. We can then create an $m \times n$ matrix of coefficients

$$\mathbf{C} = \begin{bmatrix} | & | & & | \\ \vec{c_0} & \vec{c_1} & \ldots & \vec{c_n} \\ | & | & & | \end{bmatrix}. \tag{3}$$

Finally, we introduce a vector of correction strengths, $\vec{x}$, of length n. We can then readily formulate the correction objective: find $\vec{x}$ such that

$$\mathbf{C}\vec{x} = -\vec{e}. \tag{4}$$

There is typically no exact solution and so a linear least squares method is used to solve for $\vec{x}$.

This method to set the currents in the correction circuits has been verified with numerical models. The Fourier coefficient of the radial field error after correction are shown in Fig. 6. The vertical and horizontal components of magnetic field in the center and at the edge of the cooling region are shown in Fig. 7. The field quality on-axis is bellow 1×10^{-4} in the central 1 m of the drift. The field quality within a radius of 30 mm, the radius of the electron beam with a 5 mm radial margin for steering, is bellow 2×10^{-4} in the central 0.95 m of the drift. In the horizontal dipole corrector closest to the TF region, there is margin for the correction of random error up to 1.5×10^{-3} and above 5.4×10^{-3} in all other circuits.

Simulations comparing the horizontal emittance for AD electron cooling at the 300MeV c^{-1} with a field quality of 1×10^{-3} and 5×10^{-4} are presented in [11]. In the current AD cycle, the 300MeV c^{-1} cooling plateau is 16s long. In the simulations, a comparable horizontal emittance is achieved after 8s in the 5×10^{-4} case, compared to 16s in the 1×10^{-3} case. These results imply that the improved correction scheme in the new AD cooler magnet system can deliver significant operational improvements for the AD.

A novel translating flux meter measurement system that is compatible with the correction method proposed is under active development and is reported in [12], [13].

C. Electron Beam Steering

Two causes of offset between the reference trajectory and the natural election beam trajectory from the gun to the center of the drift can be observed. The first is that the central flux line of the magnet system does not exactly follow the reference trajectory along which the coils are placed. The second is that as the electrons travel through the TF they experience a centripetal force which leads to a cross drift. These effects were simulated using the beam tracking in Opera [5]. Using a sweep of electron energies, it was found that the vertical offset of the electron beam from the gun to the center of the drift without steering can be fitted by a straight line

$$\Delta y_e = m_s \beta\gamma + c_s \tag{5}$$

where β is relativistic beta, γ is the Lorentz factor, and the fitting coefficients, m_s and c_s, are -17.1 mm and 2.0 mm respectively. The systematic horizontal offset is 4.8 mm in the direction away from the center of curvature of the electron cooler. After correcting the systematic offsets, the proposed steering scheme can provide an additional deflection of at least 5.2 mm in both planes.

V. Conclusion

The design of the magnet system for the new AD electron cooler has been presented. Options for the correction of field error in electron coolers have been compared and a field correction scheme has been proposed and verified. The correction scheme is able to provide a Ø60 mm × 950 mm cooling region with a field quality better than 2×10^{-4}, and a repeatability of better than 3.3×10^{-5} when installed. This represents a significant improvement in field quality compared to the existing electron cooler that is expected to translate to an increase in the cooling performance in the AD cycle. The magnet system is under construction and will ready for installation in the last quarter of 2026.

Acknowledgment

The authors would like to thank A. Newborough for mentorship, G. Tranquille and H. Bajas for their work on the initial integration concept used as the basis for the design developed in this paper; V. Maire for supporting the mechanical design and providing the base images used in Fig. 1 and 5; D. Gamba, G. Kahari, and M. Sameed for independently verifying the design with beam dynamics simulations; C. Carli for many enlightening conversations; A. Rossi for oversight and coordination; and the AD E-cooler team for the fruitful collaboration.

REFERENCES

[1] A. Rossi et al., "Specifications and status of the new electron cooler for the CERN antiproton decelerator (AD)," in *Proc. 14th Int. Workshop Beam Cooling Relat. Top.*, Apr. 2024, vol. 2023, pp. 5–10, doi: 10.18429/JACoW-COOL2023-MOPPM1R3.

[2] A. Wolf, L. Hütten, and H. Poth, "Magnetic field measurements in the electron cooling device for LEAR," CERN, Geneva, Switzerland, Tech. Rep. CERN-EP-INT-84-01, 1984. [Online]. Available: http://cds.cern.ch/record/149879

[3] H. Danared, "Fast electron cooling with a magnetically expanded electron beam," *Nucl. Instrum. Methods Phys. Res., Sect. A*, vol. 335, no. 3, pp. 397–401, 1993, doi: 10.1016/0168-9002(93)91223-A.

[4] T. Tanabe et al., "Design of an electron cooling device for the accumulator cooler ring in MUSES project," *Nucl. Instrum. Methods Phys. Res., Sect. A*, vol. 441, no. 1, pp. 104–109, Jan. 2000, doi: 10.1016/S0168-9002(99)01118-3.

[5] Opera 2021 SP2 Build 4, Dassault Systems U.K. Ltd., Warwick, U.K., 2021, TOSCA solver. [Online]. Available: https://www.3ds.com/products/simulia/opera

[6] G. Tranquille, A. Bubley, V. Parkhomchuk, V. Prieto, and R. Sautier, "LEIR electron cooler status," in *Proc. AIP Conf. Proc.*, Mar. 2006, vol. 821, no. 1, pp. 57–64, doi: 10.1063/1.2190093.

[7] G. Tranquille, L. Jørgensen, D. Luckin, and R. Warner, "The CERN-ELENA electron cooler magnetic system," in *Proc. 9th Int. Part. Accel. Conf.*, Jun. 2018, no. 9, pp. 842–845, doi: 10.18429/JACoW-IPAC2018-TUPAF056.

[8] J. Leibfritz et al., "Fermilab electron cooling project: Engineering aspects of cooling section," in *Proc. 2001 Part. Accel. Conf.*, 2001, vol. 2, pp. 1414–1416, doi: 10.1109/PAC.2001.986698.

[9] L. Zhao et al., "Magnet design of the electron cooling system for HIAF," *IEEE Trans. Appl. Supercond.*, vol. 32, no. 6, Sep. 2022, Art. no. 4100105, doi: 10.1109/TASC.2022.3146820.

[10] V. N. Bocharov, A. V. Bublei, S. G. Konstantinov, V. M. Panasyuk, and V. V. Parkhomchuk, "Precision measurements and compensation for the transverse components of the solenoids' magnetic field," *Instrum. Exp. Techn.*, vol. 48, no. 6, pp. 772–779, Nov. 2005, doi: 10.1007/s10786-005-0139-2.

[11] D. Gamba, A. Rossi, G. Russo, and P. Kruyt, "Specifications for a new electron cooler of the antiproton decelerator at CERN," in *Proc. 14th Int. Part. Accel. Conf.*, May 2023, no. 14, pp. 2241–2244, doi: 10.18429/JACoW-IPAC2023-TUPM027.

[12] M. Pentella, V. M. Mattsson Kjellqvist, C. Petrone, S. Russenschuck, and L. von Freeden, "Alignment of a solenoid system by means of a translating-coil magnetometer," *IEEE Trans. Appl. Supercond.*, vol. 34, no. 5, Aug. 2024, Art. no. 9001404, doi:10.1109/TASC.2024.3361430.

[13] C. Petrone, S. Sorti, E. Dalane, B. Mehl, and S. Russenschuck, "Induction-coil measurement system for normal- and superconducting solenoids," *IEEE Trans. Appl. Supercond.*, vol. 32, no. 6, Sep. 2022, Art. no. 9000605, doi: 10.1109/TASC.2022.3147142.